Nano Today 61 (2025) 102616

Contents lists available at ScienceDirect

Nano Today

journal homepage: www.elsevier.com/locate/nanotoday

Extreme environment-resistant high performance triboelectric nanogenerator for energy harvesting and self-powered positioning system

Yangjiu Zhao [a,1], Haoran Yu [a,1], Ruirui Cao [a,b,d,*], Ying Liu [a], Shaowei Shen [a], Xin Li [a], Haoyi Wu [a], Dequan Sun [a,c], Haihui Liu [c,**], Caofeng Pan [b,**]

[a] Henan Key Laboratory of Quantum Materials and Quantum Energy, School of Future Technology, Henan University, Kaifeng 475004, China
[b] Institute of Atomic Manufacturing, International Research Institute for Multidisciplinary Science, Beihang University, Beijing 100191, China
[c] School of Material Science and Engineering, Tiangong University, Tianjin 300387, China
[d] Engineering Research Center for Nanomaterials, Henan University, Kaifeng 475004, China

ARTICLE INFO

Keywords:
Triboelectric nanogenerator
Extreme environment
Durability
Thermal stability
Self-powered positioning

ABSTRACT

Ensuring the effectiveness of triboelectric devices under extreme environmental temperatures is essential for the global implementation of TENG-driven self-powered electronics in various regions worldwide, but achieving this is substantial challenging. In this work, a thermally stable and flexible PVDF-HFP/SEBS (PH_SS_O) composite membrane doped with stearic acid (SA) and octanoic acid (OA) is constructed by the method of electrostatic spraying-assisted electrospinning. Compared with the original PHS membrane, the PH_SS_O membrane not only exhibits enhanced triboelectric output (V_{oc}, I_{sc}, and Q_{sc} increased by 61.48 %, 77.11 %, and 46.16 % respectively), but also maintains a relatively stable triboelectric output from room temperature to a high-temperature environment of 60°C, highlighting its remarkable reliability and stable power supply capability. Furthermore, the fabricated $PH_{S1.5}S_{O1.5}$ triboelectric membrane exhibits outstanding hydrophobicity, flexibility, stretchability, and cyclic stability. These qualities render $PH_{S1.5}S_{O1.5}$ based TENG to be an appealing self-powered positioning device, offering critical data such as time and location to adventurers and scientists operating in extreme Earth environments, thereby ensuring their safety. In summary, this study has developed a triboelectronegative fibrous membrane materials with excellent overall performance, which to some extent ensures the effective operation of TENG-driven self-powered devices in extreme temperature environments, providing good feasibility and successful case for applications in energy harvesting and human-machine interaction fields under harsh environments.

Introduction

Triboelectric nanogenerator (TENG), based on the coupling effect of contact electrification and electrostatic induction, can convert minuscule, low-frequency and random mechanical energy into valuable electrical energy, gaining considerable attention in recent years [1–4]. This technology not only holds great promise for energy harvesting but also serves as a versatile platform for the development of wearable self-powered electronic products [5–8]. As widely acknowledged, the environmental temperature on Earth where humans reside is subject to fluctuations. It has been documented that the highest recorded temperature on Earth can reach approximately 57.7°C, which was observed in Death Valley National Park situated in California. However, most of the previous research on TENGs has been conducted at room temperature (around 25°C), neglecting the impact of temperature variations on the electrical performance of TENGs [9–11]. Despite notable advancements achieved thus far, this technology still encounters challenges when it comes to its application in demanding environments [12–17]. Therefore, developing triboelectric devices capable of effectively operating in harsh environmental conditions and determining their potential as a global sustainable power source is crucial to enabling the widespread application of TENG-driven self-powered electronic

* Corresponding author at: Henan Key Laboratory of Quantum Materials and Quantum Energy, School of Future Technology, Henan University, Kaifeng 475004, China.
** Corresponding authors.
E-mail addresses: rrcao0403@vip.henu.edu.cn (R. Cao), liuhaihui@tjpu.edu.cn (H. Liu), pancaofeng@buaa.edu.cn (C. Pan).
[1] These authors contributed equally.

https://doi.org/10.1016/j.nantod.2024.102616
Received 12 October 2024; Received in revised form 11 November 2024; Accepted 22 December 2024
Available online 26 December 2024

products in various regions worldwide.

As human exploration of the Earth deepens, electronic devices are increasingly required to possess outstanding adaptability and stable electrical output performance in extreme environments [18]. Firstly, for triboelectric devices, the output performance of the triboelectric functional layer is severely affected by environmental temperatures due to the thermionic emission effect of tribo-charges [14,19,20]. Maintaining stable electrical output of triboelectric devices over a wide temperature range is therefore an important research topic. Compared to typical metal and inorganic tribo-materials, polymer tribo-materials (PTMs) possess advantages such as material diversity, exceptional flexibility, stretchability, extensibility, and lightweight properties [21–24]. Consequently, PTMs have undoubtedly become the foundational cornerstone of TENG technology. Recent efforts have been reported aiming to enhance the operational temperature of PTM-based TENGs. Although these PTM-based TENGs can function stably at high temperatures, their electrical output is significantly lower than at room temperature due to continuous thermionic emission effects [14,24]. For instance, polyvinyl alcohol (PVA) and PVA/10 wt% PPA-PEI (phenyl phosphonic acid-branched polyethyleneimine) based TENGs can only maintain 62.8 % and 90.4 % partial efficiency, respectively, at a high temperature of 60℃ [25]. The polytetrafluoroethylene (PTFE)-coated cotton fabric-based TENGs, PTFE-based TENGs, as well as PTFE and nylon 66-based TENGs only retain output efficiencies of 91.8 % (at 60℃) [26], 65.8 % (at 55℃) [27], and 81.1 % (at 60℃) [28], respectively. Secondly, high temperatures can pose serious health risks to the human body [29,30]. Prolonged exposure to high-temperature environments can lead to heatstroke, heat exhaustion, and even heat-related injuries [31,32]. For adventurers working in outdoor high-temperature environments, the ability to immediately obtain accurate location information in case of danger is crucial to ensuring their personal safety [33]. Henceforth, the development of a TENG-driven self-powered positioning system with stable power supply holds significant research value in addressing these challenges.

Herein, electrospinning was employed for poly(vinylidene fluoride-*co*-hexafluoropropylene) (PVDF-HFP), and simultaneously, electrospraying was applied to poly[styrene-*b*-(ethylene-*co*-butylene)-*b*-styrene] (SEBS) to construct a tribo-negative composite nanofiber membrane with excellent stretchability and hydrophobicity. The SEBS elastomer functions as a microsphere adhesive between PVDF-HFP nanofibers, securely immobilizing them in distributed positions and facilitating reversible sliding during stretching to significantly enhance the stretchability. Meanwhile, building on our previous research [34–36], varying amounts of stearic acid (SA) and octanoic acid (OA) were introduced into PVDF-HFP and SEBS respectively to further improved the triboelectric characteristic of the PVDF-HFP/SEBS (PHS) composite membrane. Compared with the original PHS membrane, the V_{oc}, I_{sc}, and Q_{sc} of the as-fabricated SA and OA doped PHS (PH_SS_O) composite membrane exhibited a significant enhancement of 61.48 %, 77.11 %, and 46.16 %, respectively. Correspondingly, the dielectric constant of the corresponding PH_SS_O composite membrane is increased by 1.26 times at the frequency of 1 kHz. It is worth noting that the triboelectric output of the PH_SS_O composite membrane remains essentially unchanged from room temperature to a high-temperature environment of 60℃, highlighting its remarkable stability. Moreover, the brightness of the illuminated LEDs light exhibits consistent levels under varying temperature conditions, showcasing its reliable and stable power supply capability. This innovative PHsSo triboelectric composite membrane also exhibits excellent thermal stability, flexibility, and cyclic stability, making it an attractive self-powered positioning device for workers in Earth environments with extreme temperature, ensuring their personal safety. The study presents an effective approach for preparing nanofiber membrane-based tribo-negative materials with excellent comprehensive performance, providing promising feasibility and successful cases for applications in energy harvesting and human-machine interaction fields under extreme environments.

Experimental section

Preparation of PH_SS_O membrane

As shown in Fig. 1a, solution A was by adding varying mass fractions (*i.e.*, 0, 0.5, 1.0, 1.5 and 2.0 wt%) of SA to a 24 wt% PVDF-HPF/DMF solution, and solution B was formulated by incorporating different mass fractions (*i.e.*, 0, 0.5, 1.0, 1.5 and 2.0 wt%) of OA to a 12 wt% SEBS (G1650, Kraton) solution in a toluene and DMF mixture (mass ratio 4:1). Subsequently, solutions A and B were separately loaded into syringes, and the composite nanofiber membranes were spun by electrospinning assisted electrospraying with three needles simultaneously. The specific experimental conditions were a voltage of 16 kV, an advancing rate of 1 mL/h, a receiving distance of 18 cm, and a receiving time of 2 h. Afterwards, the obtained composite membranes were dried at 60℃ for 1 h in an oven to obtain the desired $PH_{Sx}S_{Oy}$ composite nanofiber membrane for this study. In this context, the subscripts *x* and *y* represent the mass fractions of SA and OA respectively within solutions A and B.

It is important to note that, prior to preparing the SA and OA doped PHS composite nanofiber membrane, this study systematically investigated the usage ratio of solution A and solution B in three syringes during the preparation process of the original PHS membrane. Specifically, solutions A and B were loaded into three syringes in different ratios (0:3, 1:2, 2:1, 3:0), resulting in corresponding membranes labeled as 3S, 2SP, S2P, and 3 P.

Self-powered positioning system

The prepared PH_SS_O membrane, aluminum foil and copper foil were cut to 4.5 × 4.5 cm^2 dimensions and assembled into single-electrode mode TENG. Those TENG units, along with a 470 μF capacitor, were respectively employed as power source and energy storage capacitor to ensure the uninterrupted operation of the global positioning system (GPS). Specifically, the LTC3588 module was chosen to capture the electrical outputs from the TENG devices and reliably deliver a 3.6 V voltage to the ATGM336H-5N GPS module.

Characterization

The surface morphology and element distribution of the $PH_{Sx}S_{Oy}$ composite membrane were analyzed using a field emission scanning electron microscope (JSM-7001F, JEOL, Japan). The triboelectric output of the single-electrode mode $PH_{Sx}S_{Oy}$ based TENG (4.5 ×4.5 cm^2) were measured by using a programmable electrometer (Keithley 6514, USA) at a working frequency of 1 Hz, and the moving distance of the TENG device (50 mm) was controlled by a linear motor (R-LP3, Nanoinstrument, China). The dielectric constant and dielectric loss of the samples were measured within the frequency range of 40–10^6 Hz using a TZDM-RT-1000 dielectric spectrometer. The chemical composition of the samples was analyzed by attenuated total reflection-Fourier transform infrared (ATR-FTIR, BRUKER OPTICS, Germany) measurement. The thermal stability of the samples was evaluated with thermogravimetric analyzer (TGA, TGA/DSC3+, Mettler Toledo, Switzerland) at a heating rate of 10 ℃ min^{-1}.

Results and discussion

PVDF-HFP stands out for its robust electronegativity, hydrophobicity, and high chemical stability, rendering it a widely utilized as a triboelectric functional layer [37,38]. SEBS, on the other hand, exhibits excellent elasticity, stretchability, and biocompatibility [39,40]. Considering the significance of deformable high-performance triboelectric functional layers for portable and wearable TENG devices, this study employs electrospray technology to apply SEBS elastomer as microsphere adhesive between PVDF-HFP electrospun nanofibers, which can effectively fix the PVDF-HFP nanofibers in their distributed

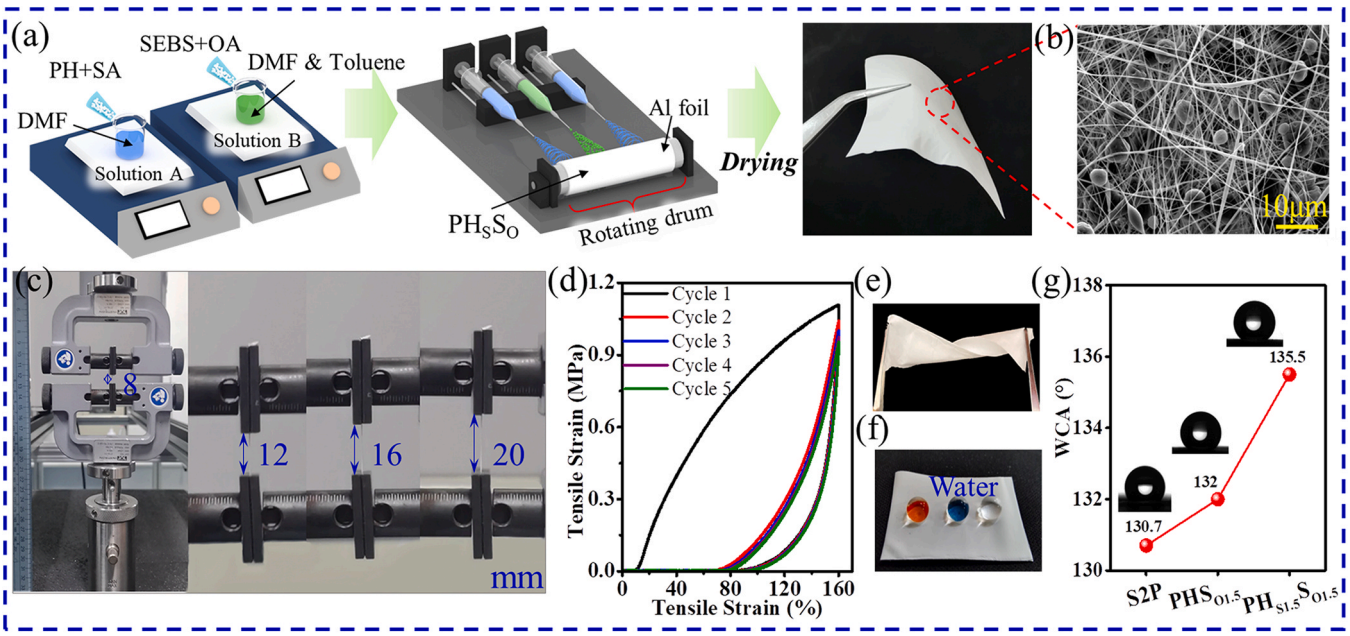

Fig. 1. Fabrication procedure, morphology characterization and mechanical property of PH_SS_O membrane. (a) Fabrication procedure and optical image of PH_SS_O membrane. (b) SEM image of $PH_{S1.5}S_{O1.5}$ membrane. (c) Photographs of $PH_{S1.5}S_{O1.5}$ sample at varying strains. (d) Cyclic stress-strain curve of $PH_{S1.5}S_{O1.5}$ sample. (e) Photographs of $PH_{S1.5}S_{O1.5}$ sample under bending and twisting conditions. (f) Photographs of water droplets on the surface of $PH_{S1.5}S_{O1.5}$ sample. (g) Water contact angle (WCA) of several typical composite membranes fabricated in this study.

positions while facilitating reversible sliding during stretching. Consequently, stretchable PH_SS_O membranes were successfully fabricated, as illustrated in Fig. 1a. From the SEM image of Fig. 1b, it can be observed that in the $PH_{S1.5}S_{O1.5}$ membrane (as a typical example of the as-fabricated PH_SS_O membranes), PVDF-HFP nanofibers are effectively anchored by SEBS microspheres, resulting in a rough surface and a

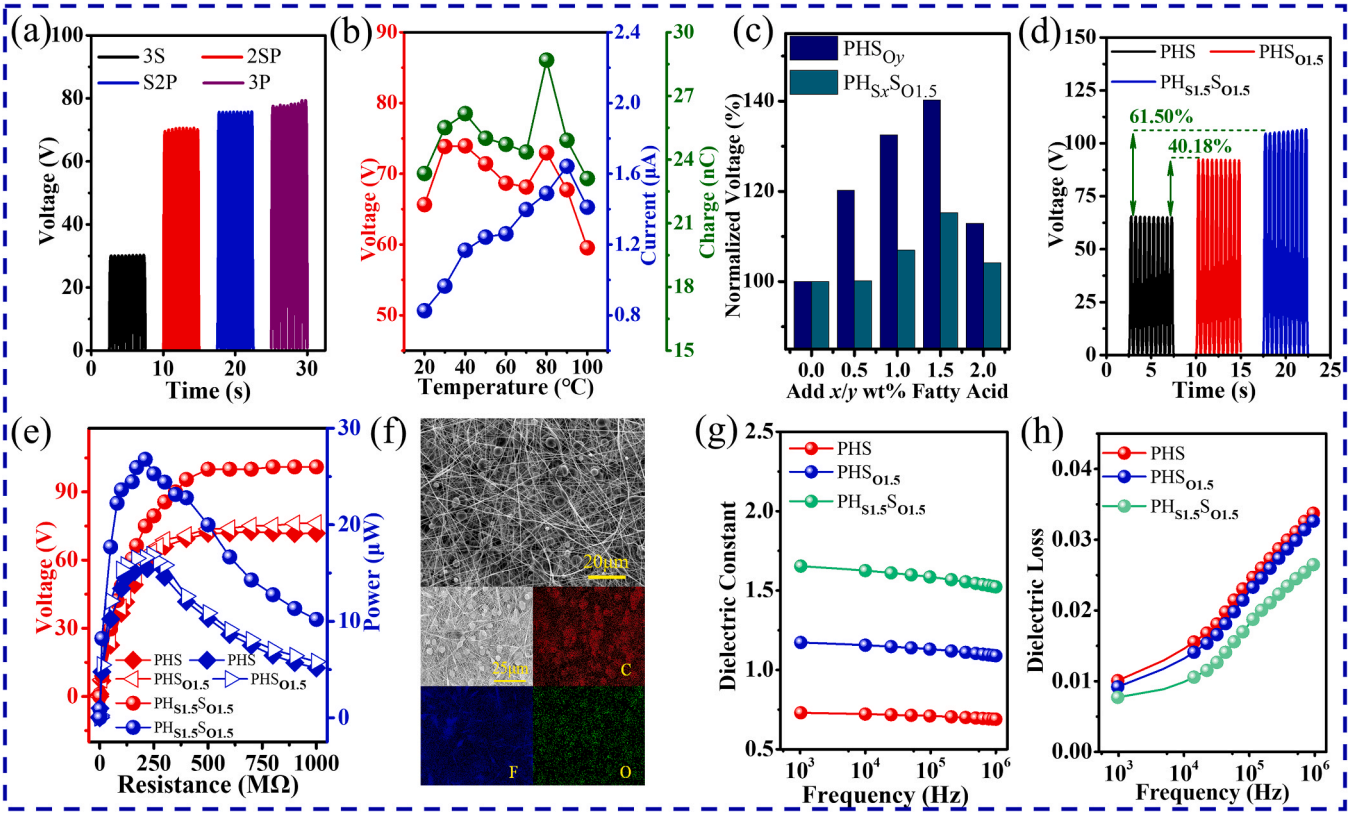

Fig. 2. Triboelectric output property of single-electrode mode a series of composite nanofiber membrane based TENGs. (a) V_{oc} of 3S, 2SP, S2P and 3 P based TENGs. (b) Temperature dependency of the electrical output (V_{oc}, I_{sc} and Q_{sc}) of PHS based TENG. (c) Normalized voltage of PHS_{Oy} and $PH_{Sx}S_{O1.5}$ membranes. (d) V_{oc} and (e) electric power of PHS, $PHS_{O1.5}$ and $PH_{S1.5}S_{O1.5}$ based TENGs. (f) Surface SEM and corresponding EDS mapping images of $PH_{S1.5}S_{O1.5}$ membrane. (g) Dielectric constant and (h) dielectric loss of PHS, $PHS_{O1.5}$ and $PH_{S1.5}S_{O1.5}$ membranes.

stable anchoring structure. This anchoring structure leverages the soft elastomer SEBS to absorb more energy under strain, buffering stress effectively [41]. Consequently, it finely regulates the distribution of tensile stress on PVDF-HFP nanofibers, imparting the PH_SS_O membrane with high tensile strength, deformability, and great recovery on cyclic tensile loading-unloading test (160 %), as presented in Fig. S1, and Fig. 1c-1d. Owing to the inherent thermoplasticity of SEBS material, a slight residual strain (80 %) was observed during the initial unloading cycle of PH_SS_O membrane, wherein energy dissipation occurs as a result of polymer chain disentanglement [42]. Additionally, as displayed in Fig. 1e-1g, the PH_SS_O membrane presents outstanding flexibility and hydrophobicity. The outstanding comprehensive performance of PH_SS_O membrane presents promising prospects for its application in the field of flexible wearable devices.

To achieve stretchable triboelectric materials with superior performance, an initial examination was conducted into the composition of the original PVDF-HFP/SEBS (PHS) composite nanofiber membrane. Samples were crafted using varying ratios of PVDF-HFP and SEBS, and their respective morphological characteristics are depicted in Fig. S2. Thanks to the remarkable tribo-electronegativity exhibited by PVDF-HFP, the electric output of the membranes (3S, 2SP, S2P, and 3 P) was observed to progressively intensify with an increase in the PVDF-HFP content, as clearly shown in Fig. 2a. While, the 3 P sample, comprising solely PVDF-HFP nanofibers, lacks the desired stretchability. Therefore, the S2P membrane was selected for subsequent research within this study. Unless otherwise indicated, any references to the PHS membrane specifically pertain to the S2P sample. It is noteworthy that the PHS membrane based triboelectric material demonstrates enhanced electrical output performance across a wide temperature range ($\leq$ 90℃), as evidenced by Fig. 2b and Fig. S3, highlighting its capability to ensure reliable and effective power supply in harsh environments, thereby showcasing significant potential for global applications.

The continual improvement in the electrical output performance of TENG is widely recognized as the primary driving force propelling their ongoing advancement and widespread industrialization [43–45]. The doping and compositing strategies of triboelectric materials are effective ways to efficiently inhibit the escape of triboelectric charges and enhance the charge retention capability of the triboelectric materials [46–48]. Drawing from our previous researches [34,35], introducing moderate amounts of OA and SA into SEBS and PVDF-HFP respectively not only augmented the triboelectric output of these matrices but also resulted in OA-doped SEBS and SA-doped PVDF-HFP composite materials that displayed improved triboelectric output across a wide temperature range compared to room temperature. Consequently, in this study, to further improve the triboelectric performance of PHS, a series of $PH_{Sx}S_{Oy}$ membranes were prepared. Fig. S4 illustrates the structure and working mechanism of $PH_{Sx}S_{Oy}$ based TENGs with a single-electrode mode. The corresponding results of the triboelectric test are shown in Fig. 2c and Fig. S5. As the OA doping quantity increases, the electrical output of PHS_{Oy} membrane initially rises but then starts to decrease. Specifically, at a doping level of 1.5 wt%, the electrical output peaks, representing a significant 40.18 % increase compared to that of the original PHS. From Fig. 2c and Fig. S5, utilizing the $PHS_{O1.5}$ membrane as a basis, a series of $PH_{Sx}S_{O1.5}$ membranes were prepared by doping with SA, which further boosted the triboelectric performance of PHS significantly. Among these, the $PH_{S1.5}S_{O1.5}$ membrane, doped with 1.5 wt% of both OA and SA, displayed the most optimal output performance, showing a 13.3 % increase over the $PHS_{O1.5}$ membrane. Additionally, Fig. 2d-2e and Fig. S6 present the triboelectric output and electric power of PHS, $PHS_{O1.5}$ and $PH_{S1.5}S_{O1.5}$. Remarkably, through the synergistic co-doping of OA and SA in the PHS membrane, the V_{oc} and effective power of $PH_{S1.5}S_{O1.5}$ increased by 61.50 % and 70.62 %, respectively, in comparison to that of original PHS.

The results depicted in Fig. 2f and Figs. S7-S8 convincingly demonstrate the successful doping of OA and SA into the membranes. All three membranes, PHS, $PHS_{O1.5}$, and $PH_{S1.5}S_{O1.5}$, exhibit a distinct structure where PVDF-HFP nanofibers are anchored by SEBS microspheres. Fig. 2f particularly highlights the uniform distribution of elements C, O, and F in the $PH_{S1.5}S_{O1.5}$ membrane, indicating a homogeneous dispersion of fatty acids within SEBS and PVDF-HFP matrices. This homogeneity suggests a strong compatibility between fatty acids and SEBS/PVDF-HFP substrates. It is well established that achieving a homogeneous distribution of filler within polymer triboelectric materials is a crucial factor for attaining outstanding output performance [49]. Furthermore, it is generally known that the intrinsic properties of triboelectric materials determine the output performance of TENG. Analyzing these properties helps to explore the root causes of output differences and deepen the understanding of the underlying mechanisms [50]. Among them, the dielectric constant of the triboelectric layer is the most critical factor, as it relates to the charge storage capacity and is directly proportional to the charge transfer density, ultimately determining the performance of TENG [51]. As shown in Fig. 2g-2h, with the introduction of OA and SA, the dielectric constant of the PHS, $PHS_{O1.5}$ and $PH_{S1.5}S_{O1.5}$ membranes gradually increases, while dielectric losses decrease. This trend verifies, from the perspective of the inherent characteristics of triboelectric materials [52], that $PHS_{O1.5}$ and $PH_{S1.5}S_{O1.5}$ membranes possess enhanced electrical output properties.

To thoroughly assess the electrical output performance of the $PH_{S1.5}S_{O1.5}$ based TENG (SP-TENG), a series of related tests were conducted under varying force, frequency, and deformation conditions. According to Fig. 3a-3c and Fig S9, when the frequency was maintained at 1 Hz, an increase in the applied force resulted in a gradual rise and stabilization of V_{oc}, I_{sc}, and Q_{sc}. This phenomenon is attributed to the elastic nature of the polymer triboelectric material, where the $PH_{S1.5}S_{O1.5}$ membrane exhibits an enlarged effective contact area as the applied force intensifies, thereby generating more tribo-charges and achieving higher electrical output [53,54]. However, once the maximum contact area is reached, further increments in force do not enhance the electrical output. The data presented in Fig. 3a-3c further indicates that, under a constant pressure of 20 N and a frequency varying from 1 to 5 Hz, the V_{oc} and Q_{sc} of the SP-TENG remain stable at around 101 V and 35 nC, respectively. In contrast, the I_{sc} gradually increases from 0.67 μA to 1.88 μA. This stability in V_{oc} and Q_{sc} is primarily due to the grounded electrode configuration of the single-electrode mode TENG, which ensures that changes in operating frequency do not alter the inherent properties of the triboelectric material. For I_{sc}, higher frequencies result in a shorter contact time between triboelectric layers, enhancing the charge flow rate and thus leading to a gradual increase with frequency [53,55]. In Fig. S10, the SP-TENG can maintain a nearly consistent and stable output as the $PH_{S1.5}S_{O1.5}$ membrane undergoes stretching from its original length up to 30 % elongation, fully accommodating deformations during human movement, thereby exhibiting excellent electromechanical capabilities. Additionally, as depicted in Fig. 3d, the $PH_{S1.5}S_{O1.5}$ membrane sustains over 10,000 cycles without any degradation in its output performance, suggesting its exceptional mechanical stability and the SP-TENG's outstanding durability.

Fig. 4a-4c and Figs. S11-S12 illustrate the temperature-dependent electrical outputs of $PHS_{O1.5}$ and $PH_{S1.5}S_{O1.5}$ membranes. As temperatures rise, the electrical output of $PHS_{O1.5}$ and $PH_{S1.5}S_{O1.5}$ experiences a modest increase or relative stability, eventually declining after a critical threshold is reached. This phenomenon is primarily attributed to the interplay between an increase in transferred charges and the dissipation of tribo-charges under high-temperature conditions [34,35,56]. Notably, within high-temperature environments below 60℃ (in line with the highest recorded temperatures on Earth), both $PHS_{O1.5}$ and $PH_{S1.5}S_{O1.5}$ membranes maintain effective, stable, and unwavering triboelectric outputs, comparable to room temperature conditions. To elaborate further, taking $PH_{S1.5}S_{O1.5}$ as a case study, Fig. 4d-4e reveal that the PHS membranes developed in this research exhibit outstanding thermal stability and durability at high temperatures, showcasing their significant potential for widespread applications across diverse regions

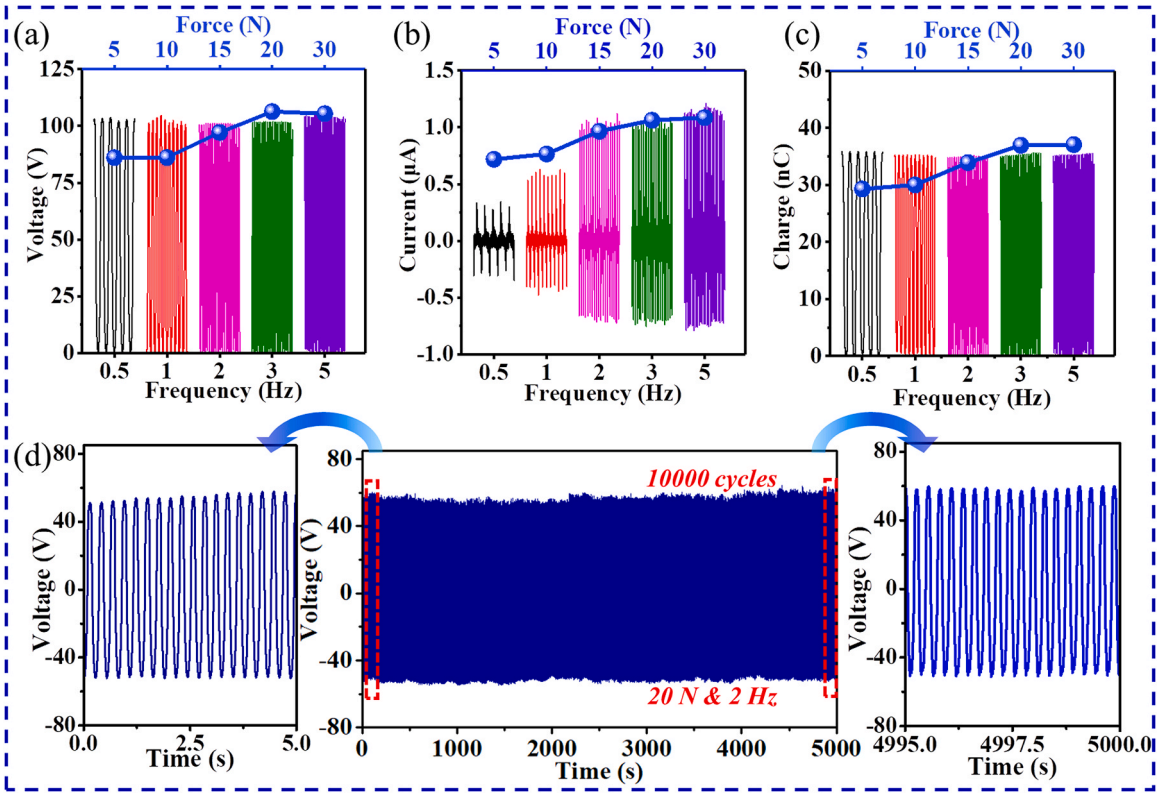

Fig. 3. Electrical output performance of $PH_{S1.5}S_{O1.5}$ membrane. (a) V_{oc}, (b) I_{sc}, and (c) Q_{sc} at different motion frequencies and pressures. (d) Output durability of the SP-TENG.

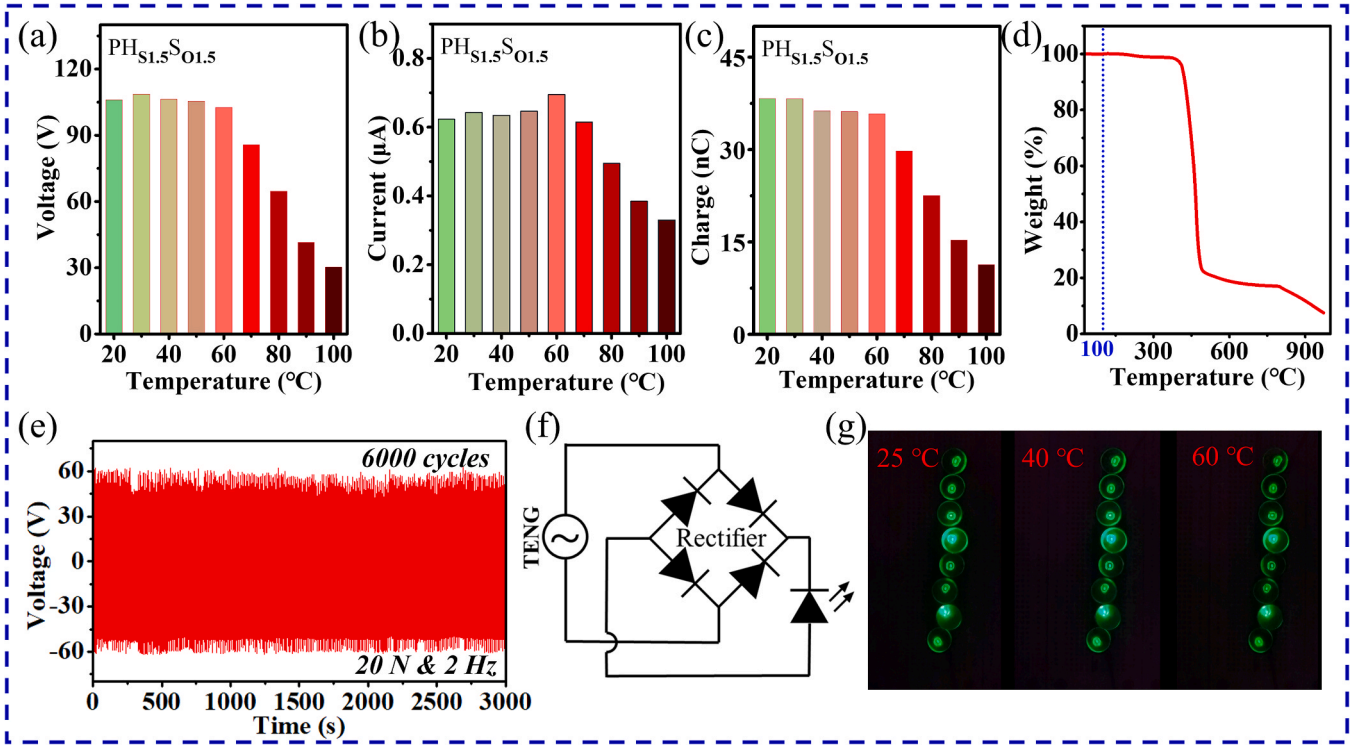

Fig. 4. Electrical outputs of $PH_{S1.5}S_{O1.5}$ membrane under various temperature conditions. Temperature-dependent (a) V_{oc}, (b) I_{sc} and (c) Q_{sc} of SP-TENG. (d) TGA curve of $PH_{S1.5}S_{O1.5}$ membrane. (e) V_{oc} of SP-TENG at 60°C before and after 6000 cycles. (f) Schematic circuit diagram of TENG for LED lighting. (g) Photographs of SP-TENG to illuminate 8 LEDs under varying temperatures.

worldwide. To demonstrate the practical utility of SP-TENG ($PH_{S1.5}S_{O1.5}$ based TENG) in high-temperature environments, relevant tests were conducted by exposing it to such conditions. The involved circuitry is depicted in Fig. 4f. The test results, as illustrated in Fig. 4g and Video S1, clearly indicate that the SP-TENG efficiently converts mechanical energy into electricity and provides a stable power source for commercial LEDs, maintaining consistent brightness even at elevated temperatures.

Supplementary material related to this article can be found online at doi:10.1016/j.nantod.2024.102616.

As mentioned above, the temperature of the Earth's environment, where humans reside, fluctuates. With the continuous deepening of human exploration of the Earth, there is an increasing demand for electronic devices to have excellent adaptability and stable electrical output performance in extreme environments [57]. Moreover, high temperature poses serious health risks to humans. Long-term exposure to high-temperature environments can lead to heatstroke, heat exhaustion, and even heat-related injuries. For scientists working in outdoor high-temperature environments, it is crucial to obtain accurate location information immediately in case of danger to ensure their personal safety [58]. Therefore, developing a self-powered positioning system driven by TENG with stable power supply is of significant research value for tracking the time and location information of workers in extreme environments. Fig. 5a-5c illustrate that the SP-TENG installed at different positions on the human body, such as the arm, leg, and shoe, can harvest mechanical energy from various human movements and continuously convert it into electrical energy, which can then power the positioning module to track the time and location information of explorers in high-temperature environments. Fig. 5d depicts a schematic diagram of the self-powered wireless positioning system based on SP-TENG. The power management circuit is crucial for optimizing the energy harvesting device. Here, the output of the SP-TENG is collected by the LTC3588 and stored in a 470 μF capacitor, stabilizing at 3.6 V. When the voltage of the storage capacitor reaches 5 V, which is the operating voltage of the ATGM336H-5N positioning module, the positioning module immediately begins searching for satellite signals and transmits the information to a computer, as shown in Fig. 5e. The charging and discharging curve of the storage capacitor is depicted in Fig. 5f. Once the positioning module starts operating, it continuously sends the received information to the computer for processing. Fig. 5f and Video S2 demonstrate the computer interface successfully achieving the positioning function. This work provides a convenient solution and practical operational example for the efficient and stable operation of self-powered electronic devices driven by TENGs in extreme environments.

Supplementary material related to this article can be found online at doi:10.1016/j.nantod.2024.102616.

Conclusion

In summary, this study has developed a thermally stable and flexible $PH_{S1.5}S_{O1.5}$ triboelectric composite membrane based TENG (SP-TENG), designed for energy harvesting and self-powered positioning systems suited to extreme environments. By refining the proportions of OA in SEBS and SA in PVDF-HFP, significant enhancements in the electrical outputs of the SP-TENG have been achieved. More precisely, compared to that of original PHS, the V_{oc} and effective power of $PH_{S1.5}S_{O1.5}$ increased by 61.50 % and 70.62 %, respectively. Remarkably, the triboelectric output of the SP-TENG maintains consistency from room temperature up to 60℃, highlighting its exceptional thermal stability, durability, and reliable power supply capability across diverse temperatures. Additionally, the innovative $PH_{S1.5}S_{O1.5}$ triboelectric membrane also showcases outstanding hydrophobicity, flexibility, and stretchability, rendering it an attractive option as a self-powered positioning system delivering invaluable data such as time and location for adventurers and scientists operating in extreme temperature Earth environments, thereby ensuring their personal safety. This study offers an

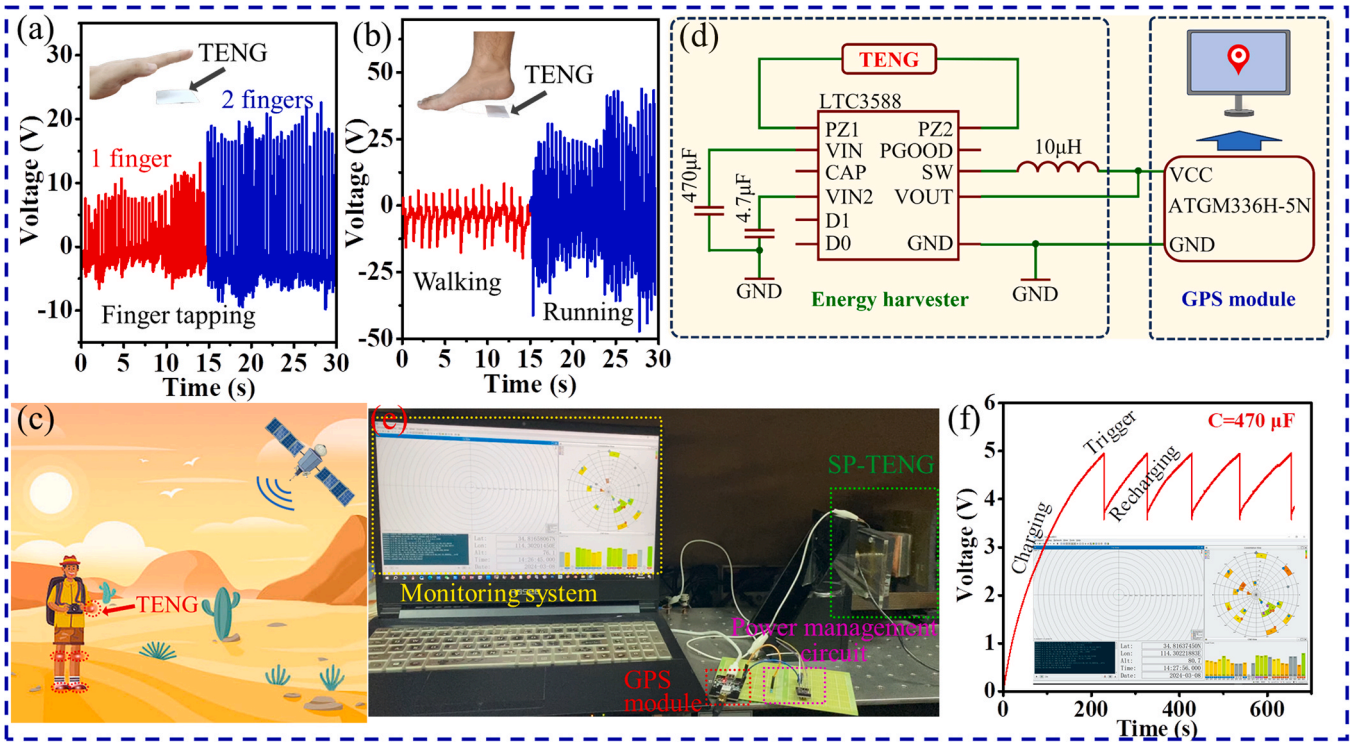

Fig. 5. Wearable smart self-powered devices. (a) and (b) Electrical signals generated by the SP-TENG during different human body motion states. (c) Conceptual diagram of SP-TENG converting human motion energy into electrical energy for self-powered wireless positioning system. (d) Schematic illustration of driving the wireless positioning system through SP-TENG. (e) A simulated test image showcasing wireless positioning capabilities in a laboratory environment. (f) Charging curve of the 470 μF commercial capacitor to drive the GPS module, and the positioning success interface displayed on the computer.

effective approach for fabricating nanofiber membrane-based tribo-negative materials with superior comprehensive performance, opening up promising avenues for energy harvesting and human-machine interaction, especially in challenging environments.

CRediT authorship contribution statement

Yangjiu Zhao: Writing – original draft, Methodology. **Haoran Yu:** Methodology, Investigation. **Ruirui Cao:** Writing – review and editing, Supervision, Resources, Methodology, Investigation. **Ying Liu:** Supervision. **Shaowei Shen:** Investigation. **Xin Li:** Investigation. **Haoyi Wu:** Visualization. **Dequan Sun:** Visualization, Investigation. **Haihui Liu:** Writing – review and editing, Supervision. **Caofeng Pan:** Writing – review and editing, Supervision, Resources.

Declaration of Competing Interest

The authors declare that they have no known competing financial interests or personal relationships that could have appeared to influence the work reported in this paper.

Acknowledgements

This work was supported by the National Natural Science Foundation of China (No. 52003074, 52125205, U20A20166 and 52192614), Postdoctoral Fellowship Program of CPSF (No. GZC20230681), National key R&D program of China (2021YFB3200300), Postdoctoral Research Foundation of Henan Provincial (HN2024058), China Postdoctoral Science Foundation (2023M741001), Natural Science Foundation for Young Scientists of Henan Province (242300421434), Natural Science Foundation of Beijing Municipality (Z180011 and 2222088) and the Fundamental Research Funds for the Central Universities.

Appendix A. Supporting information

Supplementary data associated with this article can be found in the online version at doi:10.1016/j.nantod.2024.102616.

Data availability

Data will be made available on request.

References

[1] X. Li, J. Tao, X. Wang, J. Zhu, C. Pan, Z.L. Wang, Adv. Energy Mater. 8 (2018) 1800705.
[2] L. Liu, J. Li, Z. Tian, H. Wu, S. Zhou, X. Chen, Y. Zhu, X. Yang, W. Ou-Yang, Nano Today 57 (2024) 102379.
[3] H. Zhou, C. Zhao, Z. Zhao, J. Jiang, H. Jin, S. Wang, S. Pan, M. Xu, Y. Chen, H. Jin, Rare Met. 43 (2024) 1186–1196.
[4] S. Hajra, A.M. Padhan, B.K. Panigrahi, P. Pakawanit, Z. Jagličić, N. Vittayakorn, Y. K. Mishra, S. Lee, H.J. Kim, J. Mater. 10 (2024) 792–802.
[5] C. Pan, W. Guo, L. Dong, G. Zhu, Z.L. Wang, Adv. Mater. 24 (2012) 3356–3361.
[6] J. Jia, Y. Zhu, P. Das, J. Ma, S. Wang, G. Zhu, Z.-S. Wu, J. Mater. 9 (2023) 1242–1262.
[7] J. Lai, Y. Ke, Z. Cao, W. Xu, J. Pan, Y. Dong, Q. Zhou, G. Meng, C. Pan, F. Xia, Nano Today 43 (2024) 101437.
[8] H. Zhang, D. Zhang, D. Wang, Z.-Y. Xu, Y. Yang, B. Zhang, Rare Met. 41 (2022) 3117–3128.
[9] D. Jiang, M. Lian, M. Xu, Q. Sun, B.B. Xu, H.K. Thabet, S.M. El-Bahy, M.M. Ibrahim, M. Huang, Z. Guo, Adv. Compos. Hybrid. Mater. 6 (2023) 57.
[10] J. Chai, G. Wang, J. Zhao, G. Wang, C. Wei, A. Zhang, G. Zhao, Nano Res. 17 (2023) 1942–1951.
[11] J.-H. Zhang, Z. Zhou, J. Li, B. Shen, T. Zhu, X. Gao, R. Tao, X. Guo, X. Hu, Y. Shi, L. Pan, ACS Mater. Lett. 4 (2022) 847–852.
[12] Q. Guan, X. Lu, Y. Chen, H. Zhang, Y. Zheng, R.E. Neisiany, Z. You, Adv. Mater. 34 (2022) 2204543.
[13] H. He, J. Liu, Y. Wang, Y. Zhao, Y. Qin, Z. Zhu, Z. Yu, J. Wang, ACS Nano 16 (2022) 2953–2967.
[14] X. Tao, S. Li, Y. Shi, X. Wang, J. Tian, Z. Liu, P. Yang, X. Chen, Z.L. Wang, Adv. Funct. Mater. 31 (2021) 2106082.
[15] X. Zhong, P. Sun, R. Wei, H. Dong, S. Jiang, J. Mater. Chem. A 10 (2022) 15080–15088.
[16] Y. Shao, B. Luo, T. Liu, C. Cai, X. Meng, S. Wang, S. Nie, Mater. Today 66 (2023) 348–370.
[17] K. Sun, F. Wang, W. Yang, H. Liu, C. Pan, Z. Guo, C. Liu, C. Shen, ACS Appl. Mater. Interfaces 13 (2021) 50368–50380.
[18] Y. Li, Y. Guo, F. Fu, Z. Yang, Y. Ling, J. Liu, W. Gong, Adv. Mater. 36 (2024) 2401359.
[19] C. Xu, A.C. Wang, H. Zou, B. Zhang, C. Zhang, Y. Zi, L. Pan, P. Wang, P. Feng, Z. Lin, Z.L. Wang, Adv. Mater. 30 (2018) 1803968.
[20] A.C. Wang, B. Zhang, C. Xu, H. Zou, Z. Lin, Z.L. Wang, Adv. Funct. Mater. 30 (2020) 1909384.
[21] M. Shanbedi, H. Ardebili, A. Karim, Prog. Polym. Sci. 144 (2023) 101723.
[22] X. Tao, X. Chen, Z.L. Wang, Energy Environ. Sci. 16 (2023) 3654–3678.
[23] C. Chen, S. Zhao, C. Pan, Y. Zi, F. Wang, C. Yang, Z.L. Wang, Nat. Commun. 13 (2023) 1391.
[24] R.A. Shaukat, S. Ameen, Q.M. Saqib, M.Y. Chougale, J. Kim, S.R. Patil, M. Noman, H.K. Kim, J. Bae, J. Mater. Chem. A 11 (2023) 14800–14808.
[25] X. Chen, A. Yusuf, J.S. del Rio, D.-Y. Wang, Nano Energy 81 (2021) 105656.
[26] R. Cheng, K. Dong, L. Liu, C. Ning, P. Chen, X. Peng, D. Liu, Z.L. Wang, ACS Nano 14 (2020) 15853–15863.
[27] X. Xie, Y. Zhang, C. Chen, X. Chen, T. Yao, M. Peng, X. Chen, B. Nie, Z. Wen, X. Sun, Nano Energy 65 (2019) 103984.
[28] C. Rodrigues, M. Kumar, M.P. Proenca, J. Gutierrez, R. Melo, A. Pereira, J. Ventura, Nano Energy 72 (2020) 104682.
[29] K.L. Ebi, A. Capon, P. Berry, C. Broderick, R. de Dear, G. Havenith, Y. Honda, R. S. Kovats, W. Ma, A. Malik, N.B. Morris, L. Nybo, S.I. Seneviratne, J. Vanos, O. Jay, Lancet 398 (2021) 698–708.
[30] J. Liu, B.M. Varghese, A. Hansen, Y. Zhang, T. Driscoll, G. Morgan, K. Dear, M. Gourley, A. Capon, P. Bi, Lancet Planet. Heath 6 (2022) e484–e495.
[31] G.P. Kenny, O. Jay, Compr. Physiol. 3 (2013) 1689–1719.
[32] L.R. Leon, A. Bouchama, Compr. Physiol. 5 (2015) 611–647.
[33] X. Zhao, X. Zhang, Z. Sun, P. Wang, IEEE Access 6 (2018) 13191–13199.
[34] S. Shen, Y. Zhao, R. Cao, H. Wu, W. Zhang, Y. Zhu, K. Ren, C. Pan, Nano Energy 110 (2023) 108347.
[35] Y. Zhao, S. Shen, R. Cao, H. Wu, H. Yu, X. Li, W. Zhang, C. Pan, Nano Energy 114 (2023) 108654.
[36] R. Cao, Y. Xia, J. Wang, X. Jia, C. Jia, S. Zhu, W. Zhang, X. Gao, X. Zhang, ACS Appl. Mater. Interfaces 13 (2021) 41657–41668.
[37] Y. Wang, Q. Yang, Y. Li, L. Peng, C. Zhang, S. Cheng, Y. Han, X. Cao, ACS Energy Lett. 9 (2024) 2231–2239.
[38] P. Manchi, M.V. Paranjape, S.A. Graham, A. Kurakula, L.K. Lee, V.S. Kavarthapu, J. S. Yu, Adv. Funct. Mater. (2024) 2400371.
[39] A. Šutka, K. Mālnieks, L. Lapčinskis, P. Kaufelde, A. Linarts, A. Bērziņa, R. Zābels, V. Jurķāns, I. Gorņevs, J. Blūms, M. Knite, Energy Environ. Sci. 12 (2019) 2417–2421.
[40] A. Poudel, N. Karode, P. McGorry, P. Walsh, J.G. Lyons, J. Kennedy, S. Matthews, A. Coffey, Compos. Part B 165 (2019) 397–405.
[41] Y. Li, J. Xiong, J. Lv, J. Chen, D. Gao, X. Zhang, P.S. Lee, Nano Energy 78 (2020) 105358.
[42] Y. Zhao, S. Shen, X. Wang, R. Cao, X. Jia, X. Niu, H. Liu, X. Zhang, Energy Build. 285 (2023) 112933.
[43] R. Cao, Y. Liu, H. Li, Z. Shen, F. Li, X. Jia, C. Chen, R. Liu, C. Luo, W. Yang, R. Bao, C. Pan, SusMat (2024) e196.
[44] S. Lv, X. Zhang, T. Huang, H. Yu, Q. Zhang, M. Zhu, ACS Appl. Mater. Interfaces 13 (2021) 2566–2575.
[45] Z. Liu, S. Lin, P. Yang, S. Qin, J. Hu, X. Chen, Energy Environ. Sci. 17 (2024) 6582–6593.
[46] X. Tao, P. Yang, Z. Liu, S. Qin, J. Hu, Z.-X. Huang, X. Chen, J.-P. Qu, ACS Nano 18 (2024) 4467–4477.
[47] Q.M. Saqib, I. Ahmad, A. Mannan, J. Mahmood, S. Ameen, C.S. Patil, M. Noman, J. Kim, M.S. Okyay, S.R. Patil, Y. Ko, H.-J. Noh, B.M. Wong, B.S. Kim, J. Bea, J.-B. Baek, Adv. Mater. 36 (2024) 2311029.
[48] Z. Abbas, A.P.S. Prasanna, M. Anithkumar, T.S. Bincy, N. Hussain, S.-J. Kim, S. M. Mobin, Nano Energy 132 (2024) 110344.
[49] Y. Zhang, M. Wu, Q. Zhu, F. Wang, H. Su, H. Li, C. Diao, H. Zheng, Y. Wu, Z. L. Wang, Adv. Funct. Mater. 29 (2019) 1904259.
[50] D. Zhang, W. Yang, W. Gong, W. Ma, C. Hou, Y. Li, Q. Zhang, H. Wang, Adv. Mater. 33 (2021) 2100782.
[51] Y. Yu, H. Li, D. Zhao, Q. Gao, X. Li, J. Wang, Z.L. Wang, T. Cheng, Mater. Today 64 (2023) 61–71.
[52] Z. Peng, X. Xiao, J. Song, A. Libanori, C. Lee, K. Chen, Y. Gao, Y. Fang, J. Wang, Z. Wang, J. Chen, M.K.H. Leung, ACS Nano 16 (2022) 20251–20262.
[53] M. Cheng, X. Liu, Z. Li, Y. Zhao, X. Miao, H. Yang, T. Jiang, A. Yu, J. Zhai, Chem. Eng. J. 468 (2023) 143800.
[54] X. Cao, C. Ye, L. Cao, Y. Shan, J. Ren, S. Ling, Adv. Mater. 35 (2023) 2300447.
[55] L. Feng, Z.L. Wang, X. Cao, L. Zhang, Nano Today 49 (2023) 101760.
[56] B. Cheng, Q. Xu, Y. Ding, S. Bai, X. Jia, Y. Yu, J. Wen, Y. Qin, Nat. Commun. 12 (2021) 4782.
[57] F. Jiang, X. Zhou, J. Lv, J. Chen, J. Chen, H. Kongcharoen, Y. Zhang, P.S. Lee, Adv. Mater. 34 (2022) 2200042.
[58] Z. Wang, G. Liu, J. Gao, X. Fu, B. Fan, Y. Qin, Z. Wang, Z. Zhang, Y. Chen, C. Zhang, Adv. Mater. Technol. 8 (2023) 2300487.